Global Biogeochemical Cycles

RESEARCH ARTICLE
10.1029/2020GB006702

The Importance of the Phytoplankton "Middle Class" to Ocean Net Community Production

Lauren W. Juranek[1], Angelicque E. White[2,3], Mathilde Dugenne[2,3], Fernanda Henderikx Freitas[2,3], Stephanie Dutkiewicz[4], Francois Ribalet[5], Sara Ferrón[2,3], E. Virginia Armbrust[5], and David M. Karl[2,3]

[1]College of Earth, Ocean, and Atmospheric Sciences, Oregon State University, Corvallis, OR, USA, [2]Department of Oceanography, University of Hawai'i at Mānoa, Honolulu, HI, USA, [3]Daniel K. Inouye Center for Microbial Oceanography: Research and Education, Honolulu, HI, USA, [4]Department of Earth, Atmospheric, and Planetary Sciences, Massachusetts Institute of Technology, Cambridge, MA, USA, [5]School of Oceanography, University of Washington, Seattle, WA, USA

Abstract The net balance between photosynthesis and respiration in the surface ocean is a key regulator of ocean-atmosphere carbon dioxide (CO_2) partitioning, and by extension, Earth's climate. The slight excess of photosynthesis over community respiration in sunlit waters, known as net community production (NCP), sets the upper bound on the sequestration of carbon via biologically mediated export. Prevailing paradigms suggest a high/low binary where net primary production (NPP), NCP, and export are highest in ecosystems characterized by microplankton (>20 μm) and lowest in ecosystems dominated by picoplankton (<2 μm). This bifurcation model neglects the potential importance of nanoplankton (2–20 μm)—i.e., the "middle" size class—toward global biological pump functioning. Here, we show a relationship between the biomass of nanoplankton and oxygen-based estimates of NCP across natural ecological gradients in the North Pacific Ocean. Using a suite of high-resolution optical imaging approaches including SeaFlow, Imaging FlowCytobot, and laser-based scattering, nanoplankton dynamics are observed to dominate the particle size distribution throughout an ~1,000 km transition between the subtropical and subpolar North Pacific, where NCP rates are threefold to fivefold higher than subtropical values. Based on ecological theory applied to the Darwin size-based ecosystem model, we hypothesize that intermediate size class organisms are capable of high rates of production via an optimization of bottom-up and top-down control inherent to the "middle class." More broadly, the model indicates the global importance of nanoplankton for ocean biological production.

Key Points:
- We observe elevated rates of net community production (NCP) across the North Pacific subtropical-subpolar transition zone
- Variation in NCP is strongly correlated with the biomass of cells in the "middle" size class (2–20 μm) commonly referred to as nanoplankton
- Global coupled model results suggest that nanoplankton play an important role across many high nutrient supply regions of the ocean

Correspondence to:
A. E. White,
aewhite@hawaii.edu

Citation:
Juranek, L. W., White, A. E., Dugenne, M., Henderikx Freitas, F., Dutkiewicz, S., Ribalet, F., et al. (2020). The importance of the phytoplankton "middle class" to ocean net community production. *Global Biogeochemical Cycles*, *34*, e2020GB006702. https://doi.org/10.1029/2020GB006702

Received 6 JUN 2020
Accepted 19 NOV 2020
Accepted article online 25 NOV 2020

Lauren W. Juranek and Angelicque E. White contributed equally to this work.

1. Introduction

In the ocean as on land, the size of a living cell sets critical bounds for the growth, resource acquisition, metabolic rate, and predator-prey interactions of organisms (Finkel et al., 2009; Sheldon et al., 1972; West et al., 1997). Since the original classification of Sieburth et al. (1978) partitioned phytoplankton into picoplankton (0.2–2.0 μm), nanoplankton (2.0–20 μm), and microplankton (20–200 μm), the temporal and spatial variability of phytoplankton community cell size has been used to understand ecosystem structure and function in the ocean (Chisholm, 1992). Empirical allometric relationships frequently play a central role in modeling trophic structure and the ocean's biological pump from remote sensing observations (Brewin, Sathyendranath, et al., 2010; Laws et al., 2000; Mouw et al., 2016; Siegel et al., 2014) and more recently in ecosystem models of the ocean (Dutkiewicz et al., 2020; Ward et al., 2012). Emerging from ecological frameworks relating phytoplankton size to functional type dominance under nutrient-deplete or nutrient-replete conditions (Eppley & Peterson, 1979; Margalef, 1979), long-standing paradigms of oceanic export equate high rates of net primary production (NPP) with large phytoplankton size classes and high sinking fluxes of particulate organic carbon (POC) into the ocean interior (Eppley & Peterson, 1979; Laws et al., 2000) while smaller phytoplankton are associated with low NPP, nutrient regeneration (the microbial loop), and diminished carbon export (Legendre & Le Fèvre, 1995; Michaels & Silver, 1988). Such views are further supported by assumptions regarding the effect of mineral ballasting associated with large microplankton size classes (typically diatoms).

The threshold between "large" and "small" has varied in individual studies. An early food web model by Michaels and Silver (1988) that included picoplankton, nanoplankton, and microplankton drew a functional distinction for large cells as the >20-μm microplankton size class. Legendre and Le Fèvre (1995) proposed a small/large bifurcation of primary producers, with cells <5 μm (termed "ultraplankton") driving the microbial loop and "larger cells (e.g., diatoms)" accounting for much of the export production. In this bifurcation the classical definition of the nanoplankton size class (2–20 μm) straddled the divide between small and large fractions. In more recent work building on the bifurcation approach, either a >20 μm threshold (Siegel et al., 2014) or a variable threshold (>5 μm or >20 μm) (DeVries & Weber, 2017) has been used. The implicit assumption in all of these models is that the particle size distribution (PSD) can be reduced to an ecologically meaningful binary where "large" cells preferentially drive net community and export production.

However, a growing body of evidence from field-based studies has suggested that a simple large/small binary relationship between phytoplankton size, NPP, and POC export is not adequate in many cases (cf. Richardson, 2019, and references therein). These studies include both high-latitude regimes classically thought to be dominated by microplankton and low-latitude regions dominated by picoplankton. For example, using surface dissolved O_2 and O_2 isotope budgets, Cassar et al. (2015) found that some of the highest rates of gross primary and net community production (GPP and NCP, respectively) in the sub-Antarctic zone of the Southern Ocean occurred where diatoms were minimal or absent and where picoplankton and nanoplankton communities dominated (as constrained via pigment and flow cytometry observations). In a separate study at the Western Antarctic Peninsula Long-Term Ecological Research study site, similar gas-based rate observations along with a network analysis of plankton diversity gleaned from 18S ribosomal DNA sequencing suggested complex relationships among NCP, GPP, and the phytoplankton community that were not well correlated to the presence/absence of diatoms (Huang et al., 2012; Lin et al., 2017). These studies implicated the role of trophic interactions and "top-down" forcing as important factors that introduce nuance into relationships among available nutrients, community structure, productivity, and ultimately POC export in these regions. More recently, Bolaños et al. (2020) observed that picoplankton and nanoplankton dominate high biomass communities during the onset of the North Atlantic spring bloom, in stark contrast to the classical expectation that large microplankton (specifically, diatoms) drive seasonal pulses in production in this region (Laws et al., 2000; Savidge et al., 1995).

Studies in lower latitude oceans provide additional support for a nonbinary relationship between size, production, and export. While these regions have generally been regarded to be low productivity and low export owing to low nutrient supply, dominance by picoplankton communities, efficient microbial recycling of scarce resources, and slow direct settling rates for phytoplankton cells, emerging views indicate a more substantial contribution of "small" cells (i.e., not microplankton) toward both relative and absolute production and export (Richardson, 2019). For example, in a network analysis of metagenomes collected from the global Tara Oceans survey, Guidi et al. (2016) found that diatoms occupied a surprisingly low percentage (~6%) of nodes associated with high carbon flux (determined via optical imaging with a Underwater Vision Profiler (UVP)); furthermore, dinoflagellates tended to have higher importance in the network regression. In the subtropical Atlantic at the Bermuda Atlantic Time Series site, an inverse analysis of size-fractionated pigment and ^{234}Th-based export has also suggested an important role for smaller plankton size classes toward export: Lomas and Moran (2011) found that picoplankton and nanoplankton both contribute significantly toward deep (~500 m) POC export in the subtropical Atlantic, with nanoplankton contributing to export roughly in equal proportion to their biomass in surface waters.

Open ocean regions dominated by picoplankton and nanoplankton cells (<20 μm) within the upper ocean make up the majority of ocean area (~96%, Brewin, Sathyendranath, et al., 2010) and hence contribute the majority of oceanic primary production (Viviani et al., 2011). However, the prevailing small/large binary of marine productivity and POC export results in an emphasis on oceanic regions dominated by microplankton (Dunne et al., 2007; Henson et al., 2012; Laws et al., 2000). Some integrated geochemical tracer data dispute an outsized role for high-latitude, microplankton-dominated communities. A comparison of annual NCP rates derived from long-term surface budgets of O_2 and dissolved inorganic carbon in low-latitude and high-latitude systems of the North Pacific indicate no significant difference between regimes dominated by small and large cells (3 ± 1 mol C m^{-2} year^{-1}, derived from $n = 4$ for subpolar and $n = 8$ for subtropical)

(Emerson, 2014). These studies emphasize the importance of the lower latitude ocean in global biological pump functioning.

New observational tools are helping to better quantify PSD throughout the global oceans, leading to the recognition that "middle"-sized cells—nanoplankton between 2 and 20 μm in the original definition of Sieburth et al. (1978)—dominate and/or contribute significantly to biomass in some high-latitude regions (Bolaños et al., 2020) and can contribute appreciably to NCP and particle flux globally (Buesseler & Boyd, 2009; Lam et al., 2011; Mouw et al., 2016). The nanoplankton size range includes a diverse suite of phytoplankton functional types, including calcifying phytoplankton such as *Emiliania huxleyi*; dinoflagellates with diverse metabolic strategies that blur the lines between autotrophy, mixotrophy, and heterotrophy (Edwards, 2019; Poulton et al., 2007; Sherr & Sherr, 2002; Worden & Not, 2008); and small diatoms (Leblanc et al., 2018). The potentially diverse functional roles of nanoplankton communities and the possibility that these communities may be associated with unique metabolic efficiencies or trophic structures (Ward et al., 2012) that lead to PSD and production relationships that fall outside the small/large binary argues for a reassessment of the role these ubiquitous cells play in the function of the biological pump in the global ocean.

A range of theories and mechanistic models have attempted to identify what controls plankton size distributions and relationships between size and ecosystem functioning, including the role of nanoplankton (e.g., Armstrong, 1999; Poulin & Franks, 2010; Ward et al., 2014). These models focus on the combination of bottom-up (i.e., nutrient driven) and top-down (i.e., grazer) controls as governing emergent properties such as the PSD and suggest a progression from picoplankton-dominated communities in the subtropics to inclusion of larger size classes in more productive regions. However, high-resolution measures of community production, particle size, phytoplankton diversity, and resource supply across large, basin-scale environmental gradients have previously not been available to test these models. Here, we apply unique observational tools for simultaneously resolving phytoplankton PSD, taxa diversity, and biological production rates (NCP) across several ecotones spanning the North Pacific Ocean basin.

2. Size-Production Relationships at an Ecological Transition Zone in the N. Pacific Ocean

Oceanic transition zones offer spatial translations of ecological successional patterns where natural gradients in resource supply structure the phytoplankton community (Margalef, 1979). As such, these regions offer unique opportunities to test theories of relationships among PSD, phytoplankton community composition, and production that have been developed using observations from more classically studied end-member systems. Importantly, these regions also offer insight into nonlinearities that may exist between picoplankton and microplankton-dominated systems as phytoplankton and associated grazer communities change in response to environmental gradients.

The North Pacific subtropical-subpolar transition zone (NPTZ) is a large, basin-scale feature marked by strong physical, chemical, and ecological gradients. Roden (1971, 1972) characterized the zone by a series of salinity fronts encountered at southern and northern boundaries (~32–42°N). While salinity features remain relatively stable across seasons, the location of other chemical and ecological fronts varies seasonally within the NPTZ. The most well-described ecological front is the transition zone chlorophyll front (TZCF), a chlorophyll feature that spans the breadth of the N. Pacific basin and is regarded as an important migratory pathway in fisheries ecology (Polovina et al., 2001). The TZCF, typically identified by a surface chlorophyll concentration of either 0.15 or 0.2 mg m^{-3}, migrates from ~32°N in winter to 42°N in summer; the position has historically been thought to be controlled by mechanisms that resupply surface waters with nutrients that vary both seasonally and interannually (Ayers & Lozier, 2010; Chai et al., 2003; Glover et al., 1994). Steep gradients in phytoplankton community structure have been observed coincident within the TZCF, with the small cyanobacterium *Prochlorococcus* dominating biomass south of the front (Church et al., 2008), and picoeukaryotes of various functional types rising in dominance at the TZCF (Juranek et al., 2012; Kavanaugh, Hales, et al., 2014). This succession of the phytoplankton community from small to larger cells behaves as expected given the increasing nutrient availability from south to north.

Previously, surveys of the NPTZ revealed a significant increase in both NPP and NCP coincident with the TZCF (Juranek et al., 2012). Importantly, production rates measured in the vicinity of the TZCF in spring and fall were 3–5 times higher than rates observed in adjacent subtropical and subpolar regions, which

suggests that the transition region is functionally distinct and not a linear intermediate between adjacent picoplankton and microplankton-dominated regimes. However, this prior work relied on discrete sampling of rates and community structure, with the latter being determined solely by flow cytometry (which generally samples picocyanobacteria <2 μm) and pigment-based approaches (which give no indication of size or diversity and are semi-quantitative due to photoacclimation). Accordingly, the functional importance of cells larger than ~2 μm on these trends remains unclear.

In spring 2016, 2017, and 2019 we conducted a detailed characterization of the NPTZ with a comprehensive suite of high-resolution observing techniques to tease apart the relationships among nutrient supply, PSD/community structure, and NCP in this region. We again find regional maxima in NCP rates associated with the TZCF as previously observed. However, we additionally find a quantitative relationship between NCP and biomass in the nanoplankton size class as measured by both laser-scattering and continuous flow imaging approaches. Global ecosystem modeling simulations are used to demonstrate the importance of nanoplankton to oceanic production. Our results also imply that efforts to model production using a large/small cell binary may lead to underestimations and that the role of nanoplankton in planktonic food webs should be more carefully considered.

3. Methods

In this study we bring together a number of state-of-the-art observing approaches to better understand fine-scale changes in community structure and productivity across physical, chemical, and ecological gradients in the NPTZ. Observations were collected on three spring/early summer transects of the region as part of the "SCOPE Gradients" program: 19 April to 4 May 2016 on the *R/V Ka'imikai-O-Kanaloa*, 25 May to 13 June 2017 on the R*/V Marcus G. Langseth*, and 9–30 April 2019 on the *R/V Kilo Moana*. To better understand the broader significance of our results, we also utilize results of the MIT Darwin ecosystem model, which includes 35 phytoplankton types spread over 16 size classes and several biogeochemical functional groups.

3.1. Particle Size, Biomass, and Nutrients

Observations of phytoplankton cell size are critical to evaluation of community structure-function relationships in the NPTZ. Here, the PSD was characterized via laser diffraction as described in White et al. (2015). Briefly, a laser diffractometer (Sequoia Scientific Inc., LISST-100X) was used to make continuous underway measurements from the ship's seawater intake at a nominal depth of 5–7 m near the bow of each vessel. For the first 10 min of every hour incoming seawater was passed through a 0.2-μm filter. This operationally dissolved blank (<0.2 μm) was used to correct whole water signals collected in the succeeding 50 min of each hour. Particle volume was estimated via inversion of forward scatter in 32 log-spaced bins, assuming spherical, homogeneous particles (Agrawal et al., 1991, 2008) and then converted to particulate carbon using the allometric scaling of Menden-Deuer and Lessard (2000). To simplify the description of the PSD, we calculate the binned carbon content in the effective size ranges of 1.25–2.05, 2.05–20.86, and 20.86–109.25 μm. The lower bound reflects the smallest size bin the LISST is capable of resolving (~1.25 μm), while the upper limit (~100 μm) is set by the region of the PSD where scattering of particles has been found to be significantly different from filtered water background measurements for oligotrophic waters (Barone et al., 2015), where rare, large particles dominate the signal (also as in Boss et al., 2018). The 100 μm threshold also allows more direct comparison to imaging flow cytometry. These size classes are referred to as 1.25–2, 2–20, and 20–100 μm, respectively, and include both living and detrital particles; data were binned to 1-min intervals. The weighted average particle size was calculated as described in White et al. (2015) assuming spherical geometry.

POC concentrations were determined on discrete water samples collected from the ship's uncontaminated seawater system and filtered onto precombusted glass fiber filters (GF/F) every ~2.5 hr using a semi-automated filtration device (based on the design of Holser et al., 2011) (2016, $n = 344$; 2017, $n = 378$, 2019, $n = 470$). POC was measured via high-temperature combustion as per the HOT protocols (http://hahana.soest.hawaii.edu/hot/methods/pcpn.html). All samples were corrected to remove dry filter blanks.

Discrete daily samples collected from the underway flow through system as well as the CTD-rosette were analyzed for nitrate plus nitrite ($NO_3 + NO_2$) and soluble reactive phosphorus (SRP, dominantly as phosphate) using a SEAL Analytical AutoAnalyzer III with high-resolution detectors following the colorimetric reactions of Strickland and Parsons (1972), and Murphy and Riley (1962), respectively. The limit of

quantification is 75 nmol L^{-1} for $NO_3 + NO_2$ and ~30 nmol L^{-1} for SRP, and the average precision was 0.4% and 0.2%, respectively. Accuracies, determined with daily analyses of Wako CSK standards, are within 2%. Low $NO_3 + NO_2$ concentrations (<0.5 μmol L^{-1}) were determined using a high-sensitivity chemiluminescent method (Foreman et al., 2016). The high-sensitivity method has a detection limit of 1 nmol L^{-1}, and the precision ranges between 0.4% at 1,000 nmol L^{-1} and 7% at 2 nmol L^{-1}.

3.2. Plankton Diversity

Changes in plankton community structure were measured on the 2017 and 2019 cruises with an Imaging FlowCytobot (IFCb) with imaging triggered on both scattering and fluorescence. The IFCb uses a combination of flow cytometric and video technology (Olson et al., 2003) to generate high-resolution images (3.2 pixels μm^{-1}) of cells and particles in the size range of about 4–100 μm at rate of one sample per ~20 min. This allows the visualization, enumeration, and measurement of cell size for several taxa including many diatoms, dinoflagellates, silicoflagellates, coccolithophores, cyanobacteria such as *Crocosphaera*, as well as microzooplankton including ciliates, radiolarians, and acantharians. Absolute detection of cells depends on cell size and fluorescence relative to instrument gain settings. We used a higher gain for both scattering (PMT-A) and fluorescence (PMT-B) in 2019 (0.8 and 0.87, respectively) relative to 2017 (0.4 and 0.5, respectively) to increase particle detection.

In both cruise transects, all imaged particles were annotated and classified in order to train a random forest algorithm, previously described by Sosik and Olson (2007) using code available via Sosik et al. (2016), also available online (http://doi.org/10.5281/zenodo.153978). Generic biovolume distributions were estimated from 2-D images using a distance map algorithm (Moberg & Sosik, 2012). Biovolumes were then converted to equivalent spherical diameter in order to estimate the PSD across geographic domains. As was done with LISST data, IFCb measurements of cell biovolume were converted to cellular C via allometric scaling (Menden-Deuer & Lessard, 2000). Image features, including size, shape, and pixel intensity, were used to automatically classify organisms spanning nearly 200 genera of the following classes: *Bacillariophyceae* (58), *Dinophyceae* (58) *Oligotrichea* (27), *Prymnesiophyceae* (16), *Acantharia* (5), *Chrysophyceae* (5), *Dictyochophyceae* (4), or *Cyanophyceae* (3). The overall out-of-bag error rate (a metric used to assess prediction error of random forest classifications) of the algorithm initially scored at 22% indicating a higher level of classification error than acceptable. To increase the accuracy of planktonic diversity, we corrected the random forest classification by manually verifying all annotations. We then tested for differences in the community composition across ecological gradients (subtropical, southern transition zone, northern transition zone) by calculating the pairwise *ß*-diversity as $ß_{Jaccard} = \frac{a}{a+b+c}$ where a is the number of shared genera between defined domains and b and c are the number of domain-specific genera for each region. Images classified as "detritus", calibration beads, bubbles, and fecal pellets were not considered in the analyses of IFCb-based biomass.

Continuous flow cytometry of surface seawater from the ship's underway flow through system was conducted via SeaFlow, which measures autofluorescing particles ranging in size from ~0.4 to ~6 μm in diameter based on forward light scatter (457/50 band-pass filter), phycoerythrin fluorescence (572/28 band-pass filter), and chlorophyll fluorescence (692/40 band-pass filter). Data are binned to 3-min intervals. A combination of manual gating and statistical methods was used to identify *Prochlorococcus* (<1 μm), *Synechococcus* (~1 μm), and picoeukaryote cells (~ > 2 μm). Diameters and carbon quotas of individual cells were estimated from SeaFlow-based light scatter by the application of Mie theory for spherical particles, calibrated using particles of known refractive indices and several phytoplankton species of known carbon content (Ribalet et al., 2019). SeaFlow's upper limit of detection was set by particles with saturated forward light scatter signals (5.7 and 6.4 μm for 2017 and 2019 cruise, respectively), which were removed from the PSD. We note that all metrics of the PSD (LISST, IFCb, and SeaFlow) have the largest uncertainties at the upper and lower limits of the detectable size ranges and hence very likely underestimate particle abundance and biovolume in these bins. This is shown in other cross comparisons of the PSD via various instruments by a tailing off of the PSD at lower size bins in particular (e.g., Lomnard et al., 2019). Acknowledging this limitation, the aim here was not specifically to assess accuracy of particle detection across instruments but to evaluate multiple measures of the PSD relative to production across a latitudinal gradient.

3.3. Production

We employed both incubation-based and in situ O_2-based approaches to measure production across the NPTZ.

3.3.1. Incubation-Based Production

Water samples for ^{14}C assimilation rate measurements (a proxy for NPP) were collected before dawn at 15 m (within the mixed layer) using polyvinyl chloride Niskin bottles mounted on a rosette. Samples were incubated in flow through deck-board incubators in 2016 and in temperature-controlled incubators in 2017 and 2019 (set to collection temperatures) which were each screened with blue filters to 55% of surface irradiance, to approximate in situ light levels assuming an attenuation coefficient of 0.04 m^{-1} (Letelier et al., 2004). In 2019, samples for incubations were collected from the ship's underway system (~7 m) prior to dawn to improve spatial resolution. Modified Hawaii Ocean Time-series protocols were used on all cruises to measure in vitro dawn to dusk PP via the ^{14}C radiotracer method (Karl et al., 1996). Detailed methods and calculations for the ^{14}C primary production method are provided in supporting information of White et al. (2017). Rate measurements in 2016–2017 light bottles were also corrected to remove the rate measured in parallel dark bottles, which were on average 3 ± 2% (n = 22) of light values. Dark incubations were not conducted in 2019.

3.3.2. Dissolved O_2/Ar and In Situ NCP

The ratio of dissolved O_2/Ar in the surface mixed layer was determined by an equilibrated inlet mass spectrometer (EIMS) as described by Cassar et al. (2009). Surface seawater was sampled from the same seawater intake as the other underway measurements. O_2/Ar was continuously monitored with a Pfeiffer Prisma quadrupole mass analyzer 220, and gas saturations were calibrated by periodically admitting uncontaminated outside air. Additional verification was provided by comparison to discrete bottle samples collected from both the underway seawater supply and near-surface Niskin bottles analyzed shore-side using a Thermo 253 isotope ratio mass spectrometer (IRMS) in dual inlet mode (Juranek & Quay, 2005, 2012; Luz & Barkan, 2000); these comparisons indicated that no further corrections were required in 2016 and 2017 as all bottle data were within propagated measurement uncertainty (±0.3%, based on standard error of repeated in-house standards extracted through the sample processing line and analyzed via IRMS) of coincident EIMS data with no evidence of bias. A small bias correction was applied to the 2019 data. Details of EIMS data quality control are available with archived data (see data availability statement for doi). Additionally, no consistent biases were observed between flow-through and surface Niskin samples (n = 6 paired comparisons in 2016, n = 5 in 2017, n = 3 in 2019) (Juranek et al., 2010). Data collected in 2016 and 2017 were binned into ~5-min time-averaged intervals. Improvement in EIMS system control (e.g., jacket-coated, heated quadrupole chamber, and improvements in secondary electron multiplier tuning) in 2019 allowed for higher-quality data binned into shorter time intervals (~3 min).

Measurements of O_2/Ar in surface seawater relative to the O_2/Ar saturation ratio give the net oxygen saturation resulting from the in situ autotrophic and heterotrophic community, which is stoichiometrically related to net organic carbon production, regardless of phase (e.g., dissolved organic carbon or POC) (Cassar et al., 2015; Juranek et al., 2012; Kaiser et al., 2005) as in the simplified photosynthesis expression, $CO_2 + H_2O \rightarrow CH_2O + O_2$. To calculate NCP rates, a steady-state mass balance between net biological production and air-sea gas exchange of oxygen was assumed, as previously described (Cassar et al., 2007; Kaiser et al., 2005):

$$NCP = kC_{sat}(\Delta O_2/Ar)$$

where k (m day^{-1}) is the air-sea gas transfer coefficient for O_2 (Wanninkhof, 2014), C_{sat} (mmol m^{-3}) is the equilibrium concentration of O_2 (García & Gordon, 1992), and ΔO_2/Ar *is the O_2/Ar saturation* with respect to solubility equilibrium expressed as follows:

$$\Delta O_2/Ar = \left(\frac{\left({}^{O_2}/_{Ar}\right)measured}{\left({}^{O_2}/_{Ar}\right)saturation} - 1 \right)$$

The simple mass balance assumes that net O_2 production (or loss) is balanced by air-sea O_2 gas exchange, with no terms for vertical O_2 supply/loss. Recent modeling work (Teeter et al., 2018) and observations

comparing cumulative short-term NCP to that calculated with the steady-state assumption reveal that these assumptions are first-order accurate (Ferrón et al., 2015). To estimate the air-sea gas transfer coefficient k, the Wanninkhof (2014) relationship between wind speed and gas transfer was used; wind speed history from the NCEP North American Regional Reanalysis (https://www.esrl.noaa.gov/psd/data/gridded/data.narr.html) for 60 days preceding the sampling date was used to calculate k, weighted by the fraction of the mixed layer ventilated each day, and then averaged for each sample location, as described by Teeter et al. (2018). NCP rates derived from the surface O_2 mass balance indicate a time-averaged NCP over the turnover timescale of O_2 in the surface mixed layer, which in this study was 10–15 days.

3.4. Ecosystem Model

To place our regional observations in a broader oceanic context, we evaluate the importance of cell size toward biomass and production using a global ecosystem model. The biogeochemical-ecosystem model is modified from Dutkiewicz et al. (2020) and resolves the cycling of carbon, phosphorus, nitrogen, silica, iron, and oxygen through inorganic, living, dissolved, and particulate organic phases. The biogeochemical and biological tracers are transported and mixed by the MIT general circulation model (MITgcm) (Marshall et al., 1997) in a global 1° horizontal resolution configuration which is constrained to be consistent with altimetric and hydrographic observations (Wunsch & Heimbach, 2007). The ecosystem component is modified from Dutkiewicz et al. (2020) only in number of phytoplankton types and in how the phytoplankton's growth responds to temperature. In Dutkiewicz et al. (2020) many plankton types had constrained temperature ranges; here all types respond to temperature following an Arrhenius curve (Kooijman, 2000) such that growth is higher at warmer temperatures. This model includes 35 phytoplankton types describing several functional groups of phytoplankton (picophytoplankton, coccolithophores, diazotrophs, diatoms, and mixotrophic dinoflagellates) distributed over 16 size classes (from an Equivalent Spherical Diameter [ESD] of 0.6 to over 200 μm).

This simulation uses Monod kinetics and a C:N:P:Fe stoichiometry that is constant over time (though differs between phytoplankton groups). Parameters influencing growth, grazing, and sinking are related to size and parameterized as a power function of cell volume following syntheses of laboratory results (e.g., Litchman et al., 2007; Menden-Deuer & Lessard, 2000; Mongin et al., 2006; see also discussion in Ward et al., 2012). Maximum growth rates are parameterized as distinct between functional groups with diatoms having the highest rates (Buitenhuis et al., 2008; Dutkiewicz et al., 2020; Sommer et al., 2017; Tang, 1995). Plankton smaller than 3 μm have an increase of growth rate with size, and those larger than 3 μm have a decrease of growth rate with size. This unimodal distribution has been observed (e.g., Finkel et al., 2010; Marañón et al., 2013; Sommer et al., 2017) and explained as a trade-off between replenishing cell quotas versus synthesizing new biomass (Verdy et al., 2009; Ward et al., 2017). In particular, the fastest growing types are those in the nanoplankton range. There are 16 size classes of zooplankton that graze on plankton between 5 and 15 times smaller than themselves, though preferentially 10 times smaller. We use a Holling III function to model changes in grazing rates as a function of prey concentration (Holling, 1966).

The ecosystem model quickly (within 2 years) reaches a quasi-steady state. In the biogeochemistry, there is a slow drift as deep water nutrient distributions adjust; this would take hundreds to thousands of years for the model to reach full steady state but does not significantly change the results over the periods we examine. Here we show results from the tenth year of the simulation. The distributions of the plankton in this model compare well with both observations based on functional types as well as size distributions (Buitenhuis et al., 2013; Ward, 2015).

4. Results and Discussion

4.1. Meridional Productivity and PSD Trends in the NPTZ

Satellite-based chlorophyll a (chl) with overlaid satellite-based salinity contours illustrate the broad basin-scale patterns encountered on our three cruises transecting the North Pacific basin (Figure 1). We characterize regimes according to physical and ecological boundaries established in previous studies of this region. The boundary between the subtropical gyre and the southern edge of the transition zone is defined by the 34.82 surface isohaline (Roden, 1971). The meridional location of this isohaline was relatively constant between cruises (32.15°N, 32.5°N, 32.34°N in 2016, 2017, and 2019, respectively, Figure 1), consistent with

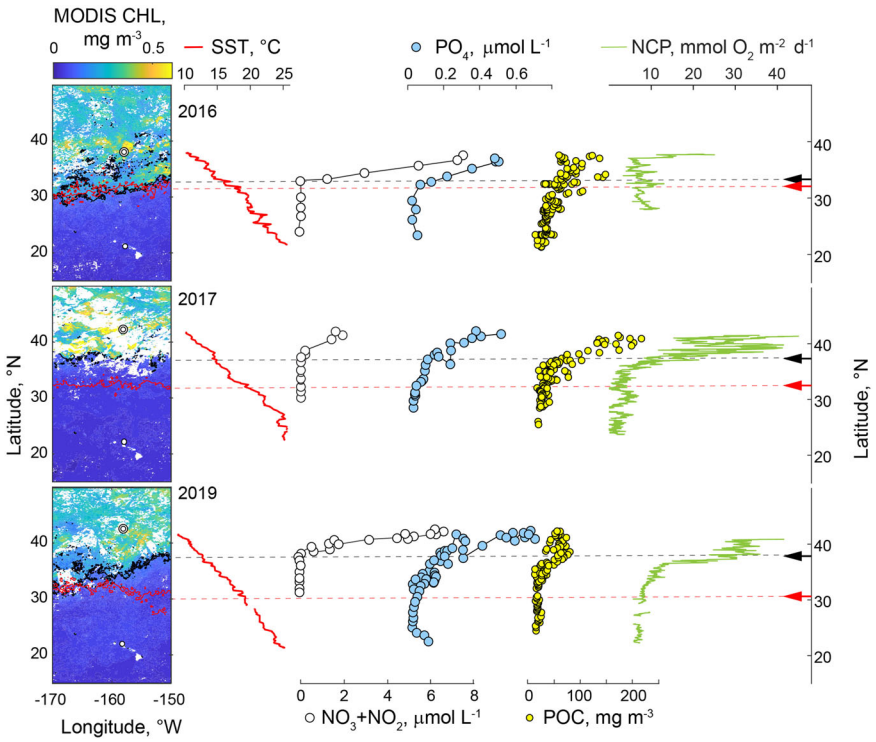

Figure 1. The April 2016 (top row), June 2017 (middle row), and April 2019 (bottom row) monthly composite of satellite-derived chlorophyll a (MODIS CHL) in the North Pacific Ocean. In all maps, the approximate location of the salinity isohaline (34.82) indicative of the southern transition zone boundary is represented by a red contour line and the 0.15 mg m^{-3} chlorophyll TZCF boundary is denoted as a black contour line. White circles on the maps indicate the northernmost latitude sampled along the 158°W meridian and the cruise origin in Honolulu, Hawaii. Adjacent panels from left to right show SST (red line), nitrate+nitrite (NO_3 + NO_2, white circles), phosphate (PO_4, blue circles), particulate organic carbon (POC, yellow circles), and net community production (NCP, green line) along the transect. Arrows at the right margin mark the latitude of the 34.82 salinity (red arrow-dashed line) and 0.15 mg m^{-3} chl front (black arrow-dashed line) for each cruise.

previous analysis (Rodin, 1971). Within the transition zone, we define a northern and southern subregion separated by the TZCF, based on the location of the 0.15 mg m^{-3} surface chlorophyll concentration (Figure 1). Considerably more variability was observed in the position of the TZCF between cruises (33.0° N, 36.2°N, 35°N in 2016, 2017, and 2019, respectively, Figure 1). While some of this variability might be expected from differences in the seasonal timing of the cruises relative to the typical northward migration of the TZCF in spring, interannual differences are also apparent (i.e., the difference between April 2016 and April 2019 TZCF location), presumably an indication of interannual differences in the large-scale physical forcing that determines nutrient availability and subsequent ecological responses.

Nutrient, productivity, and biomass data indicate several robust patterns in chemical and biological fronts observed within the transition zone (Figure 1). First, inventories of NO_3 + NO_2 and PO_4 rise, with the concentration of PO_4 increasing in the southern transition zone, slightly before a NO_3 + NO_2 increase at the TZCF. Total biomass, as approximated by both POC measurements and satellite-derived chl, increases rapidly starting at the TZCF, reaching a maximum at the northern edge of our transects. Concomitant with the biomass increase, NCP derived from continuous surface measurement of O_2/Ar indicates a threefold (2016, 2019) to fivefold (2017) increase (Figure 1). Similar magnitude changes between NCP and biomass along the transect suggest that production is driven primarily by biomass rather than a change in production per unit biomass (Figure 1). However, large uncertainties in the mixed layer volumetric NCP (i.e., NCP/MLD, mmol m^{-3}) due to variable mixed layer depth (MLD) in this weakly stratified region make it difficult to investigate metabolic efficiencies further.

Meridional NCP trends were also matched by comparable increases in incubation-based NPP rates derived from ^{14}C-assimilation (Figure 2). This suggests that higher NCP in this region was due to higher NPP and a

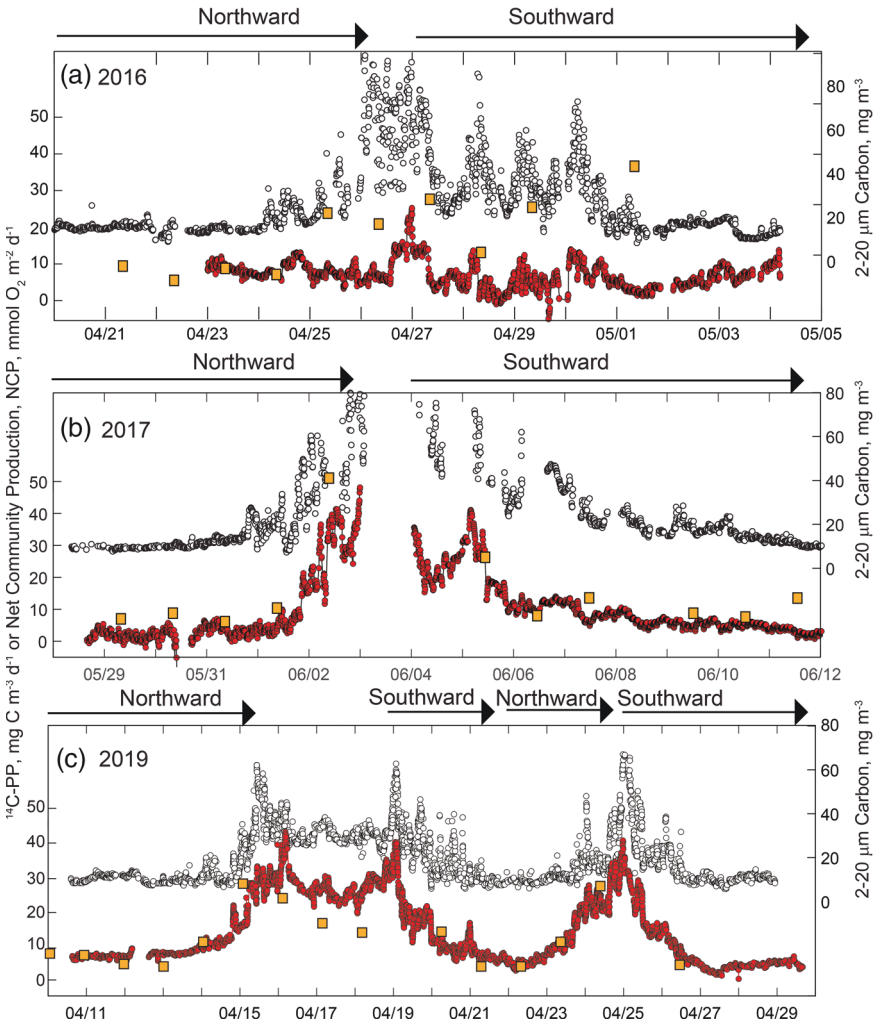

Figure 2. NCP (red circles), 12-hr ^{14}C-based primary production (orange squares) and the estimated carbon content in the 2- to 20-µm size fraction from LISST observations (white circles) with time in (a) 2016, (b) 2017, and (c) 2019. Note that in all cases cruises initiated in Honolulu, Hawaii, at ~21.3°N and transited north (see Figure 1), after which transit was due south in 2016–2017 with N-S transects in 2019.

relatively stable NCP/NPP rather than a decoupling between photosynthesis and community respiration. The ratio of NCP/NPP differed between cruises, with higher NCP/NPP observed in June 2017 and April 2019 relative to April 2016, suggesting a lower potential export efficiency in 2016.

Perhaps the most interesting observation in this comprehensive data set was a strong coherence between variation in NCP and the biomass in the 2- 20 µm "middle" size class of the LISST (Figure 2). These patterns are particularly clear when plotted versus time (as in Figure 2) rather than latitude because short-term spatial and temporal variability (i.e., while sitting on station or sampling the same latitude) obscure the relationship. This relationship between NCP and nanoplankton biomass is further explored in section 4.2.

While it is tempting to associate the increases in NCP and biomass within the northern transition zone as a gradual ecological succession into a microplankton-driven subpolar ecotype regime, the PSD from both LISST and IFCb data does not indicate this is the case (Figures 3 and 4). Instead, observations indicate that the increase in biomass in the northern transition zone is associated with a rise of plankton in the nanoplankton size class. Underway flow cytometry tuned for detection of picoplankton reveals a clear shift toward larger picoplankton (*Synechococcus* and picoeukaryotes) within the transition zone, and imaging flow cytometry tuned to nanoplankton size classes and forward scattering (LISST, here 1.25–100 µm) reveals a broadening PSD with latitude (note that the >100-µm size class accounted for ~14% of the summed POC concentration on average across cruises, again consistent with this size class being near the instrument

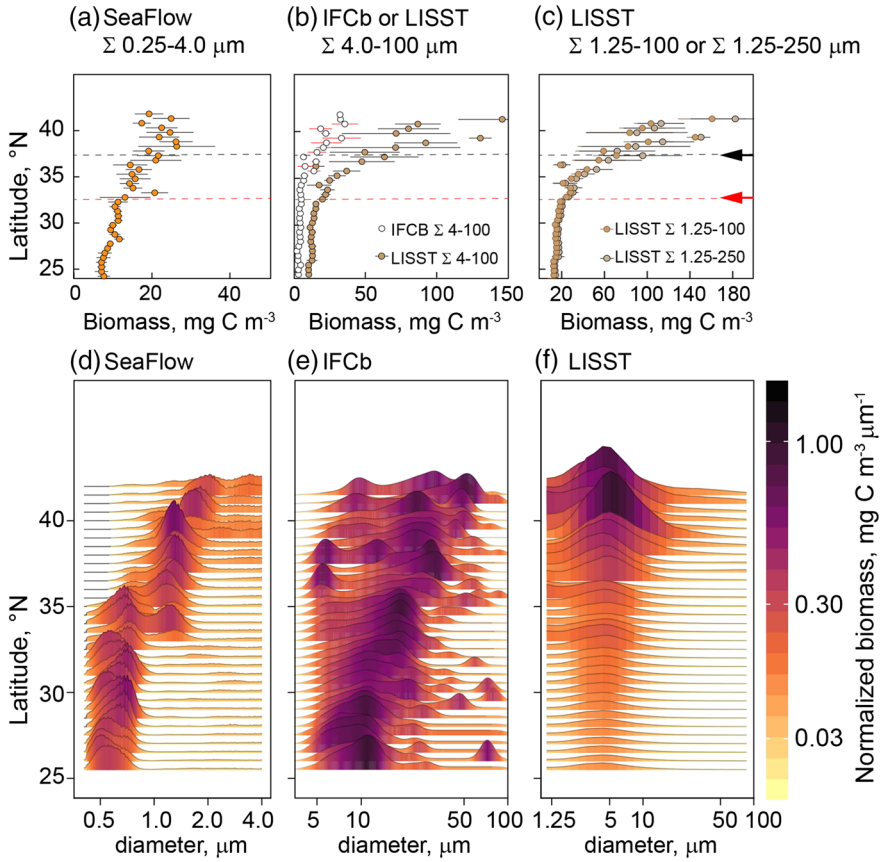

Figure 3. Total biomass as a function of latitude (binned to 0.5°) in 2017 derived from (a) underway flow cytometry, SeaFlow, in the 0.25-4.0 μm range, (b) imaging flow cytometry (IFCb) which detects particles in the ~4.0-100 μm range and forward scatter-based measurements via a LISST-100X in this same size range for comparison, and (c) LISST particle concentrations in the 1.25-100 μm range as well as the 1.25-250 μm range. As described in the methods, the >100 μm size range is near LISST detection limits and driven by large rare particles so not considered in the microplankton size class. Panel C illustrates that inclusion of this upper size range does not impact latitudinal trends. Also, note that the scale of the *x* axis differs between instruments. (d–f) Contours depict the biomass in individual size classes (binned to 0.5°) for each instrument, normalized to bin width. The height of each curve indicates biomass composition per size bin; normalized biomass concentrations are also noted by the contour color. As in Figure 1, at the right margin in panel C marks the latitude of the 34.82 salinity (red arrow-dashed line) and 0.15 mg m^{-3} chl front (black arrow-dashed line).

detection limits). Importantly, the mode of the PSD in all instruments is consistently <20 μm across the full latitudinal gradient. In 2017, we observed a significant shift in the abundance and size of particles across the meridional transect via the IFCb, with the mode of particle size shifting from 5.52 μm in the subtropics to 6.75 μm in northern transition zone waters (ANOVA, $F = 9{,}722$, $p < 0.001$) (Figure 3). We acknowledge that the mode of particle size is close to the detection limit of the instrument, which would indicate that biomass in the small-sized bins may be even higher than those reported here. In 2019, the modal size of the plankton cells appeared more similar between the subtropics and the southern transition zone, with respective modes of 7.60 and 7.45 μm, compared to the northern transition zone (6.48 μm) (Figure 4). While the partitioning of the biomass across the size classes differed between the LISST and the IFCb, likely due the fundamental difference between a scatter-based and an image-based instrument, the summed 4-100 μm carbon content between the IFCb and the LISST is in excellent agreement over the transects (r^2 of a Model 2 linear regression = 0.85 in 2017 and 0.86 in 2019, $p < 0.01$; these data are shown in Figures 3 and 4). In 2019, the IFCb biomass closely approximated the LISST 4–100 μm; in 2017 the trends were similar but the IFCb biomass was less than that of the LISST due to the lower gain setting.

The composite view of the PSD afforded by flow cytometry, IFCb, and LISST observations identifies the NPTZ as a functionally distinct ecotype between the subtropical and subpolar oceans. In this northern transition

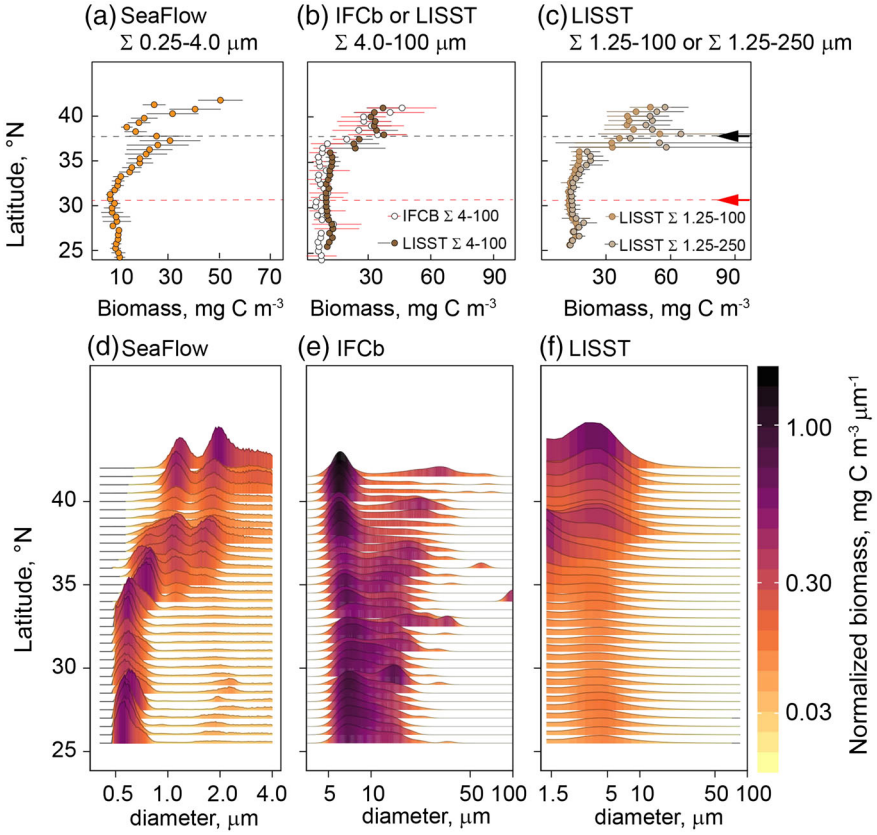

Figure 4. Total biomass as a function of latitude (binned to 0.5°) in 2019 derived from (a) underway flow cytometry, SeaFlow, in the 0.25-4.0 μm range, (b) imaging flow cytometry (IFCb) which detects particles in the ~4.0-100 μm range and forward scatter-based measurements via a LISST-100X in this same size range for comparison, and (c) LISST particle concentrations in the 1.25-100 μm range as well as the 1.25-250 μm range. As described in the methods, the >100 μm size range is near LISST detection limits and driven by large rare particles so not considered in the microplankton size class. Panel c illustrates that inclusion of this upper size range does not impact latitudinal trends. Also, note that the scale of the *x* axis differs between instruments. (d–f) Contours depict the biomass in individual size classes (binned to 0.5°) for each instrument, normalized to bin width. The height of each curve indicates biomass composition per size bin; normalized biomass concentrations are also noted by the contour color. As in Figure 1, at the right margin in panel c marks the latitude of the 34.82 salinity (red arrow-dashed line) and 0.15 mg m^{-3} chl front (black arrow-dashed line).

zone region nanoplankton dominate biomass while microplankton comprise a small proportion of cells and biomass. These observations are consistent with the predictions of the Darwin model (further discussion in section 4.3). Several lines of prior evidence also support the notion that the northern transition zone is functionally distinct from the subpolar regime. A self-organizing hierarchical clustering analysis of satellite-based sea surface temperature, salinity, height, CDOM, chlorophyll, and altimetry data in the central North Pacific identified a functionally distinct "northern transition zone" region between the TZCF and a subpolar regime at ~45°N (Kavanaugh, Emerson, et al., 2014). Moreover, surface dissolved micronutrient concentrations and nutrient amendment experiments on each cruise indicated that Fe was nonlimiting throughout the NPTZ on each survey or at least did not stimulate biomass production (data not shown). Additionally, historical analysis of the northern boundary of the NPTZ as defined by hydrography/salinity gradients suggests a boundary at ~42°N (Roden, 1971), which was only barely breached on the April 2019 transect.

4.2. A Robust Relationship Between NCP and Nanoplankton

The simultaneous high-resolution observing approaches employed here revealed a striking and robust relationship (Table 1 and Figure 2) between NCP and biomass in smaller plankton size classes, particularly the

Table 1
Model II Regression Coefficients Calculated via a Least Squares Bisector Approach for the Relationship Between C Content in picoplankton (0.2–2.0 μm), Nanoplankton (2–20 μm), and Microplankton (20–100 μm) particulate Carbon (μmol C m^{-3}) Derived From LISST, Flow Cytometry (FCM, i.e., SeaFlow for Picoplankton and IFCb for Nanoplankton/Microplankton) and the Rate of NCP Determined From O_2/Ar Observations (mmol O_2 m^{-2} day^{-1}) or Ecosystem Model Output (mg C m^{-3} day^{-1})

	LISST C content versus NCP, r	FCM C content versus NCP, r	Ecosystem model C content versus NCP_{model}, r
Size fraction	**19 April to 5 May 2016 (~22–38°N)**		
Pico, 0.2–2.0 μm	0.16 (1.25–2.0 μm)	NA	0.04 (NS)
Nano, 2.0–20 μm	0.36	NA	0.81
Micro, 20–100 μm	0.16	NA	0.78
Size fraction	**25 May to 13 June 2017 (~22–42°N)**		
Pico, 0.2–2.0 μm	0.57	0.27	0.42
Nano, 2.0–20 μm or 4.0–20 μm for IFCb	0.91	0.80	0.51
Micro, 20–100 μm	0.71	0.44	0.51
Size fraction	**9–30 April 2019 (~22–42°N)**		
Pico, 0.2–2.0 μm	0.59	0.07	0.21 (NS)
Nano, 2.0–20 μm or 4.0–20 μm for IFCb	0.86	0.51	0.87
Micro, 20–100 μm	0.35	0.11	0.84

Note. Note that NCP estimated by the ecosystem model (NCP_{model}) is defined as the difference of (NPP − grazing). The total number of paired, time-matched comparisons for LISST-NCP data was n = 1,530 (2016), n = 1528 (2017), and n = 6,245 (2019). Differences in instrument specific size classes are noted in parentheses if deviating from the operational definitions of plankton size classes. All correlations were significant with p values <0.05 unless not significant (NS) is noted. Ecosystem model output is monthly averages for the last year of a 10-year model run. IFCb data (4–100 μm) were not available (NA) for 2016.

2-20 μm nanoplankton "middle" size class. Though increases in NCP have previously been observed in the NPTZ (Juranek et al., 2012; Kavanaugh, Hales, et al., 2014; Lockwood et al., 2012), this relationship between NCP and nanoplankton in the region was previously unknown. Fine-scale coherence of trends in NCP and nanoplankton biomass is noteworthy, considering that the turnover timescale for surface O_2 (~weeks) is much longer than that of plankton biomass (~days) and short-term variability in production would tend to decouple these tracers. While the optical scattering observations of the LISST cannot distinguish living from detrital fractions of biomass, relative agreement between LISST and IFCb-based biomass indicates that these trends are driven by living cells (Figures 3 and 4).

A model II regression indicates a significant correlation between 2- 20 μm nanoplankton and NCP in the 2017 and 2019 transects (r = 0.91 with n = 1,553, r = 0.86 with n = 6,245, respectively); in 2016 a lower, but still significant, correlation is observed (r = 0.36, n = 1,530) which may be a consequence of the more limited latitudinal span (<38°N). Importantly, the correlation coefficient for the relationship between NCP and microplankton (20–100 μm) is weaker (r = 0.16, 0.71, and 0.35 for 2016, 2017, and 2019, respectively, Table 1). We also found a strong correlation between the estimated C content in the ~4- 20 μm size class detected by the IFCb and NCP rates (r = 0.80 in 2017, r = 0.51 in 2019; Table 1). These data implicate nanoplankton as important drivers of enhanced production in the low-moderate nutrient transition zone regime.

Classification of particles imaged by the IFCb indicated gradients in diversity and functional type dominance throughout the transect. The overall ß diversity significantly decreased with increasing latitude (ANOVA, F = 47.5 $p < 2.10^{-16}$), with indices in 2017/2019 of 0.64/0.63 in the subtropical gyre, 0.56/0.48 in the southern TZ, and 0.63/0.53 in northern TZ. In the subtropical gyre, where diversity was highest, rare but large cells such as the ciliate *Mesodinium* (50%) and rafts of diazotrophs including *Trichodesmium* and *Rhizosolenia* with endosymbiotic *Richelia* (between 2% and 4%) notably contributed C content (Figure 5). In the southern transition zone, gymnodinoid dinoflagellates like *Lepidodinium* (in 2017) or *Gymnodinium* (in 2019) dominated both plankton biomass and abundance (data not shown). In both years, gymnodinoid dinoflagellates contributed on average ~35% of estimated nanoplankton carbon content in the transition zone. The most abundant organism had a mean cell size of 5.44 ± 0.7 and 5.08 ± 0.46 μm in 2017 and 2019, respectively.

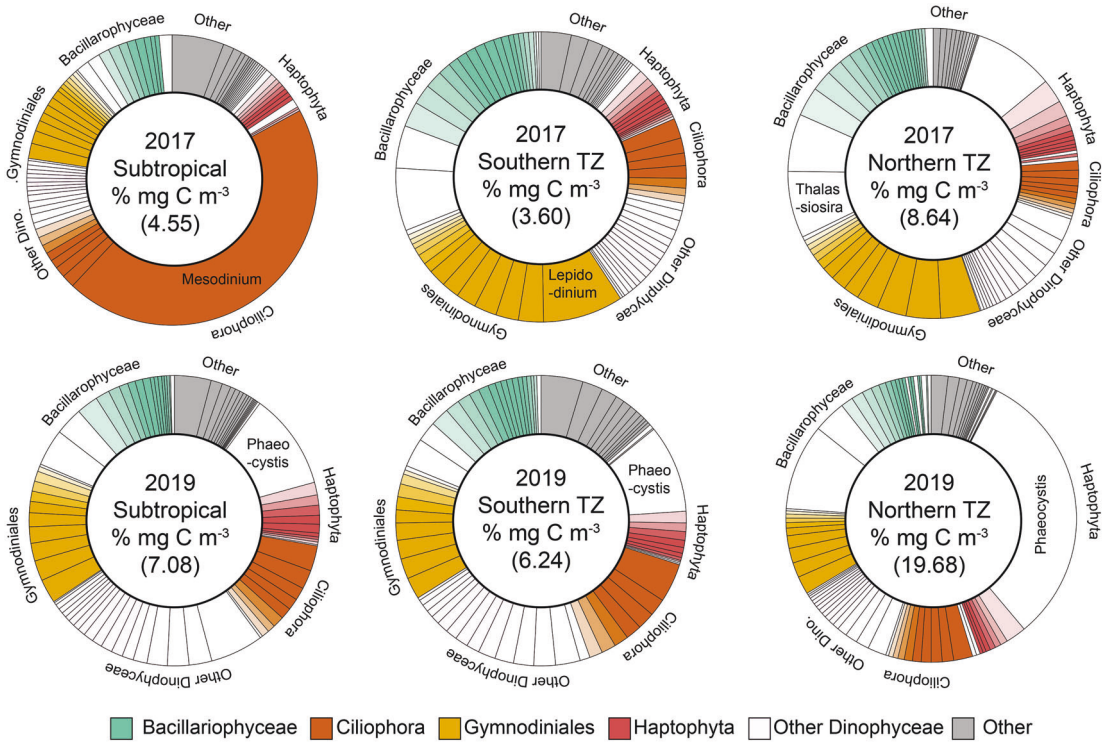

Figure 5. Relative carbon concentrations in six distinct classes of plankton including Bacillariophyceae, Ciliophora, Gymnodiniales, Haptophyta, other Dinophyceae, and other for 2017 (top) and 2019 (bottom) meridional transects as estimated via imaging flow cytometry. Community composition is shown from left to right for subtropical and southern and northern TZ regimes. In parentheses in the center of each ring is the mean carbon content in each region derived from the IFCb (~4–100 μm) and the dominant genus is noted in text. Individual "wedges" correspond to unique genera with shading from the colors denoted at the bottom.

In the northern transition zone waters, small diatoms such as the chain-forming *Thalassiosira* and coccolithophores were most abundant. Small nanoflagellates putatively associated to *Chlamydomonas* (based on size reported in Moutier et al., 2017) or *Phaeocystis* were observed across the full transect. These coordinated measurements reveal clear ecotones of phytoplankton community composition across N. Pacific transects, with the nanoplankton "middle class" detected by optical scattering and imaging flow cytometry to be dominated by dinoflagellates, coccolithophores, or even small diatoms. These patterns in particle size and cell diversity appear to strongly impact NCP and potentially export production over these same time scales.

In a recent review, Richardson (2019) outlines current evidence that supports an important role for small cells in the functioning of the ocean's biological pump. Small cells are often found to contribute in a biomass-proportionate manner toward NPP in open ocean settings where they numerically dominate. Physical aggregation of small cells, "deceptively high" sinking rates for specific nanoplankton (e.g., coccolithophorids), as well as grazing and subsequent fecal pellet production via pelagic tunicates, and appendicularians are all verified pathways for export of picoplankton and nanoplankton (Legendre & Le Fèvre, 1995; Richardson, 2019). Observations from a sediment trap deployed at 100 m in the northern transition zone in 2019 (41.5°N) revealed an export rate broadly consistent with the fourfold increase in surface NCP rate between the subtropics and northern transition zone (POC flux rate obtained from a 2.5-day deployment of 112.9 mg C m^{-2} day^{-1}, nearly fourfold higher than the long-term average at Station ALOHA of 28.1 mg C m^{-2} day^{-1}). Furthermore, aggregates containing nanoplankton as well as nonaggregated coccolithophores were observed in traps (data not shown); these findings are at least consistent with the mechanisms for picoplankton and nanoplankton export described by Richardson (2019).

Dinoflagellates may also mediate enhanced production and export via a number of mechanisms. As a functional group, dinoflagellates have large genomes and diverse trophic strategies (Hackett et al., 2004). These

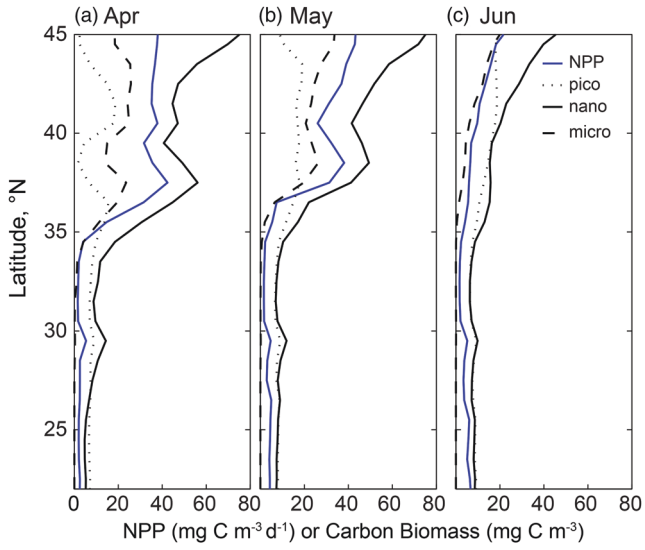

Figure 6. Net primary production (NPP) and biomass in three phytoplankton size classes (picophytoplankton, nanophytoplankton, and microphytoplankton) in the ecosystem model for (a) April, (b) May, and (c) June. Modeled data are from the surface layer (upper 10 m).

include kleptoplasty and mixotrophy, which are traits that could serve not only to potentially increase production under nutrient-limited conditions but also to enhance export production via a carbon shunt to larger grazers, as detailed in recent modeling work (Ward & Follows, 2016). Additionally, certain dinoflagellate genera, in particular *Lepidodinium* spp., have been associated with high rates of transparent exopolymer saccharide (TEP) production (Claquin et al., 2008; Passow, 2002), which could contribute significantly to enhanced aggregation. Neither our findings nor those summarized in Richardson's review (Richardson, 2019) refute the notion that microplankton contributions to community production and export can be substantial; rather our work indicates that ignoring contributions of smaller cells which may dominate production over vast swaths of oceanic basins may lead to systematic underestimation of primary and export production. We further explore this argument via a size-based ecosystem model.

4.3. Ecosystem Modeling Predicts Importance of Nanoplankton Production in the Global Ocean

To better understand the importance of observed relationships among phytoplankton size and productivity in a broader oceanic context, we evaluate the potential contributions of nanoplankton (versus picoplankton and microplankton) toward biomass and production using a global ecosystem model. The Darwin ecosystem model with 35 phytoplankton types distributed over 16 size classes captures the broad ecological and productivity patterns observed in this study; namely, it predicts a sharp increase in nanoplankton biomass across the transition zone that is closely linked with productivity (Figure 6). Model-based relationships between NCP and size-fractionated biomass support our ship-based data, suggesting a correlation between nanoplankton and community production for the same time period as the cruises (see Table 1).

Based on existing ecological theory (Armstrong, 1999; Poulin & Franks, 2010; Ward et al., 2014), the increase in nanoplankton in the transition zone is predictable. At very low nutrient supply rates, as found in the south of the transect, the smallest phytoplankton with their high nutrient affinity (due to their surface area to volume ratio, Aksnes & Egge, 1991; Pasciak & Gavis, 1975) are the best adapted and exclude larger cells. But since this small size class biomass is capped by their predator (Armstrong, 1999; Ward et al., 2014), they are unable to use the excess nutrients further north on the transect where the supply rates are much higher. Larger cells are therefore able to access these excess nutrients, and in this region nanophytoplankton can coexist with the smaller types. This succession—allowing phytoplankton of increased size to co-exist with smaller size classes with increasing nutrient supply—requires some level of size-dependent grazing. Using a similar size-structured model, Dutkiewicz et al. (2020) showed that when only a generalist grazer (i.e., one which grazed on all size classes) was included, only the smallest type of plankton in each functional group survived, dramatically reducing the size fractionation of the biomass and hence primary production. Thus, we suggest that the importance of the nanoplankton in this transition zone is caused by a combination of bottom-up processes (i.e., increased nutrient supply) and top-down, size-specific grazing.

More broadly, the size-based model predicts an important role of nanoplankton toward oceanic production (Figure 7). The model suggests that the results seen in the observations in the North Pacific Ocean are likely to be similar in many other transition regions of the ocean. Globally, over the open ocean, the model predicts that nanoplankton contribute substantially to oceanic biomass and primary production, even in high-latitude regions traditionally perceived to be dominated by microplankton (Figure 7).

5. Implications for Future Work

The role of phytoplankton functional groups and diversity in driving variation in primary and export production is a fundamental question in oceanography and carbon cycle science. While allometric approaches have been extensively used in oceanographic studies to scale particle size to metabolism, growth, and production (Brewin, Lavender, et al., 2010; Marañón et al., 2013; Uitz et al., 2008; White et al., 2015), our data and an

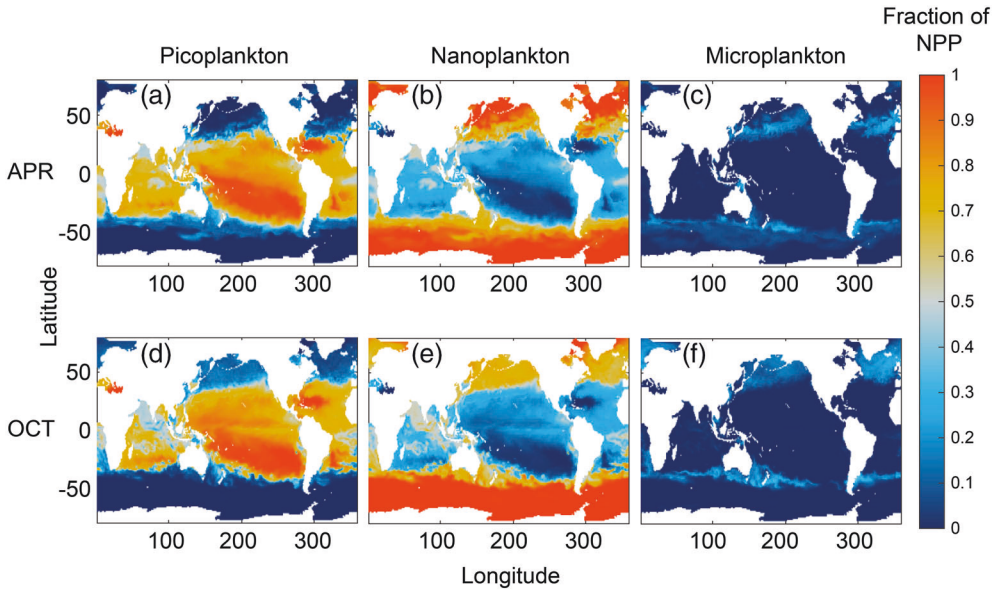

Figure 7. Fraction of ecosystem model net primary production (NPP) attributed to picoplankton (a, d), nanoplankton, (b, e), and microplankton (c, f) for April (top row) and October (bottom row).

emerging body of observational data (Bolaños et al., 2020; Fowler et al., 2020) suggest that the relationship between the PSD and production is more complex than previously thought. Both bottom-up and top-down processes, including regionally varying supply of limiting nutrients and differential grazing pressure relative to growth, are likely modes of controlling the size fractionation of the phytoplankton communities. However, there is currently little observational constraint regarding grazing rates on picoplankton and nanoplankton; this lack of data may lead to biases in the way models are constructed, with an emphasis on more simplistic models (i.e., a large/small binary) that are easier to generalize and parameterize.

As satellite-based observations and models will be required to detect baseline shifts in biological pump functioning in response to future climate forcing, there is a critical need to further evaluate relationships between PSD, NCP, and ultimately annual particle export in order to reduce uncertainty in estimates from space. An empirical relationship between chlorophyll and dominance of larger cells has been used in several algorithms that attempt to estimate size fractionation of phytoplankton globally (e.g., Brewin, Sathyendranath, et al., 2010; Hirata et al., 2011). Such studies suggest (though do not highlight) an increased importance of nanoplankton in some intermediate latitudes. Meanwhile, recent models of global export production based on remotely retrieved particle size distributions (Kostadinov et al., 2010) and biomass-based NPP (Westberry et al., 2008) have used a small/large bifurcation in a food web modeling approach to predict a biological pump export of ~6 Pg C year^{-1} (Siegel et al., 2014), roughly half that reported in prior estimates (Dunne et al., 2007; Laws et al., 2000; Schlitzer, 2000). The lower export may in part reflect model-based assumptions regarding reduced contributions of smaller phytoplankton size classes toward organic carbon production and export.

Contributions of nanoplankton to the biological carbon pump should not be neglected as algorithms to predict production and export from space are refined, particularly as these organisms dominate distributions throughout temperate regions and can substantially contribute on an area basis. Furthermore, predictions of how biological pump functioning will respond to projected warming and stratification changes under future climate forcing require understanding of how changes in nutrient supply and grazing both act to result in potential allometric shifts and functional group dominance (Laufkötter et al., 2015). Emerging capabilities to simultaneously constrain primary and net community production (e.g., with dissolved gases) and community structure via an array of high-throughput approaches including imaging flow cytometry, optical and holographic proxies, and genomic data (with appropriate caveats that genomic data give information regarding diversity but not meaningful estimates of relative abundance) will be critical for identifying and quantifying relationships between plankton size and production across ecological settings.

Data Availability Statement

All data have been uploaded to http://Zenodo.org (10.5281/zenodo.3958315; 10.5281/zenodo.4009653; 10.5281/zenodo.4079505; 10.5281/zenodo.4104636) and are freely available at the Simons Collaborative Marine Atlas Project (https://simonscmap.com/).

Acknowledgments

We are grateful for the sea-going support from marine technicians and crews of *R/V Ka'imikai-O-Kanaloa*, *R/V Marcus G. Langseth*, and *R/V Kilo Moana*, without which this work would not have been possible. We thank K. Watkins-Brandt for a wide range of technical support in 2016–2017 and T. Rohrer for technical expertise in 2019, R. Tabata for operating SeaFlow during the 2017 cruise, Karin Björkman for ^{14}C measurements in 2019, Rhea Foreman for nutrient analyses in 2018-2019 and Susan Curless in 2017, and A. Hynes for helping with the analysis of SeaFlow data and operating the instrument on the 2019 cruise. This work was primarily supported by Simons Foundation awards 329104 to A. E. W., L. W. J., E. V. A., and D. M. K. and 574495 to F. R. with additional support by National Aeronautics and Space Administration (NASA) 80NSSC17K0561 to S. D., F. R., and E. V. A.

References

Agrawal, Y., McCave, I., & Riley, J. (1991). Laser diffraction size analysis. In J. Syvitski (Ed.), *Principles, methods, and application of particle size analysis* (pp. 119–129). Cambridge, UK: Cambridge University Press.

Agrawal, Y., Whitmire, A., Mikkelsen, O. A., & Pottsmith, H. (2008). Light scattering by random shaped particles and consequences on measuring suspended sediments by laser diffraction. *Journal of Geophysical Research*, *113*, C04023. https://doi.org/10.1029/2007JC004403

Aksnes, D., & Egge, J. (1991). A theoretical model for nutrient uptake in phytoplankton, marine ecology progress series. *Oldendorf*, *70*(1), 65–72. https://doi.org/10.3354/meps070065

Armstrong, R. (1999). Stable model structures for representing biogeochemical diversity and size spectra in plankton communities. *Journal of Plankton Research*, *21*(3), 445–464. https://doi.org/10.1093/plankt/21.3.445

Ayers, J. M., & Lozier, M. S. (2010). Physical controls on the seasonal migration of the North Pacific transition zone chlorophyll front. *Journal of Geophysical Research*, *115*, C05001. https://doi.org/10.1029/2009JC005596

Barone, B., Bidigare, R. R., Church, M. J., Karl, D. M., Letelier, R. M., & White, A. E. (2015). Particle distributions and dynamics in the euphotic zone of the North Pacific Subtropical Gyre. *Journal of Geophysical Research: Oceans*, *120*, 3229–3247. https://doi.org/10.1002/2015JC010774

Bolaños, L. M., Karp-Boss, L., Choi, C. J., Worden, A. Z., Graff, J. R., Haëntjens, N., et al. (2020). Small phytoplankton dominate western North Atlantic biomass. *The ISME Journal*, *14*, 1663–1674. https://doi.org/10.1038/s41396-020-0636-0

Boss, E., Haëntjens, N., Westberry, T. K., Karp-Boss, L., & Slade, W. H. (2018). Validation of the particle size distribution obtained with the laser in-situ scattering and transmission (LISST) meter in flow-through mode. *Optics Express*, *26*(9), 11,125–11,136. https://doi.org/10.1364/OE.26.011125

Brewin, R. J., Lavender, S. J., Hardman-Mountford, N. J., & Hirata, T. (2010). A spectral response approach for detecting dominant phytoplankton size class from satellite remote sensing. *Acta Oceanologica Sinica*, *29*(2), 14–32. https://doi.org/10.1007/s13131-010-0018-y

Brewin, R. J., Sathyendranath, S., Hirata, T., Lavender, S. J., Barciela, R. M., & Hardman-Mountford, N. J. (2010). A three-component model of phytoplankton size class for the Atlantic Ocean. *Ecological Modelling*, *221*(11), 1472–1483. https://doi.org/10.1016/j.ecolmodel.2010.02.014

Buesseler, K. O., & Boyd, P. W. (2009). Shedding light on processes that control particle export and flux attenuation in the twilight zone of the open ocean. *Limnology and Oceanography*, *54*(4), 1210–1232. https://doi.org/10.4319/lo.2009.54.4.1210

Buitenhuis, E., Pangerc, T., Franklin, D. J., Le Quéré, C., & Malin, G. (2008). Growth rates of six coccolithophorid strains as a function of temperature. *Limnology and Oceanography*, *53*(3), 1181–1185. https://doi.org/10.4319/lo.2008.53.3.1181

Buitenhuis, E., Vogt, M., Moriarty, R., Bednarsek, N., Doney, S., Leblanc, K., et al. (2013). MAREDAT: Towards a world atlas of MARine Ecosystem DATa. *Earth System Science Data*, *5*(2), 227–239. https://doi.org/10.5194/essd-5-227-2013

Cassar, N., Barnett, B. A., Bender, M. L., Kaiser, J., Hamme, R. C., & Tilbrook, B. (2009). Continuous high-frequency dissolved O_2/Ar measurements by equilibrator inlet mass spectrometry. *Analytical Chemistry*, *81*(5), 1855–1864. https://doi.org/10.1021/ac802300u

Cassar, N., Bender, M. L., Barnett, B. A., Fan, S., Moxim, W. J., Levy, H., & Tilbrook, B. (2007). The Southern Ocean biological response to aeolian iron deposition. *Science*, *317*(5841), 1067–1070. https://doi.org/10.1126/science.1144602

Cassar, N., Wright, S. W., Thomson, P. G., Trull, T. W., Westwood, K. J., de Salas, M., et al. (2015). The relation of mixed-layer net community production to phytoplankton community composition in the Southern Ocean. *Global Biogeochemical Cycles*, *29*, 446–462. https://doi.org/10.1002/2014GB004936

Chai, F., Jiang, M., Barber, R. T., Dugdale, R. C., & Chao, Y. (2003). Interdecadal variation of the transition zone chlorophyll front: A physical-biological model simulation between 1960 and 1990. *Journal of Oceanography*, *59*(4), 461–475. https://doi.org/10.1023/A:1025540632491

Chisholm, S. W. (1992). Phytoplankton size. In P. G. Falkowski & A. Woodhead (Eds.), *Primary productivity and biogeochemical cycles in the sea* (pp. 213–237). New York: Springer.

Church, M. J., Björkman, K. M., Karl, D. M., Saito, M. A., & Zehr, J. P. (2008). Regional distributions of nitrogen-fixing bacteria in the Pacific Ocean. *Limnology and Oceanography*, *53*(1), 63–77. https://doi.org/10.4319/lo.2008.53.1.0063

Claquin, P., Probert, I., Lefebvre, S., & Veron, B. (2008). Effects of temperature on photosynthetic parameters and TEP production in eight species of marine microalgae. *Aquatic Microbial Ecology*, *51*(1), 1–11. https://doi.org/10.3354/ame01187

DeVries, T., & Weber, T. (2017). The export and fate of organic matter in the ocean: New constraints from combining satellite and oceanographic tracer observations. *Global Biogeochemical Cycles*, *31*, 535–555. https://doi.org/10.1002/2016GB005551

Dunne, J. P., Sarmiento, J. L., & Gnanadesikan, A. (2007). A synthesis of global particle export from the surface ocean and cycling through the ocean interior and on the seafloor. *Global Biogeochemical Cycles*, *21*, GB4031. https://doi.org/10.1029/2006GB002907

Dutkiewicz, S., Cermeno, P., Jahn, O., Follows, M. J., Hickman, A. E., Taniguchi, D. A., & Ward, B. A. (2020). Dimensions of marine phytoplankton diversity. *Biogeosciences*, *17*(3), 609–634. https://doi.org/10.5194/bg-17-609-2020

Edwards, K. F. (2019). Mixotrophy in nanoflagellates across environmental gradients in the ocean. *Proceedings of the National Academy of Sciences USA*, *116*(13), 6211–6220. https://doi.org/10.1073/pnas.1814860116

Emerson, S. (2014). Annual net community production and the biological carbon flux in the ocean. *Global Biogeochemical Cycles*, *28*, 14–28. https://doi.org/10.1002/2013GB004680

Eppley, R. W., & Peterson, B. J. (1979). Particulate organic matter flux and planktonic new production in the deep ocean. *Nature*, *282*(5740), 677–680. https://doi.org/10.1038/282677a0

Ferrón, S., Wilson, S. T., Martínez-García, S., Quay, P. D., & Karl, D. M. (2015). Metabolic balance in the mixed layer of the oligotrophic North Pacific Ocean from diel changes in O2/Ar saturation ratios. *Geophysical Research Letters*, *42*, 3421–3430. https://doi.org/10.1002/2015GL063555

Finkel, Z. V., Beardall, J., Flynn, K. J., Quigg, A., Rees, T. A. V., & Raven, J. A. (2009). Phytoplankton in a changing world: Cell size and elemental stoichiometry. *Journal of Plankton Research*, *32*(1), 119–137.

Finkel, Z. V., Beardall, J., Flynn, K. J., Quigg, A., Rees, T. A. V., & Raven, J. A. (2010). Phytoplankton in a changing world: Cell size and elemental stoichiometry. *Journal of Plankton Research*, *32*(1), 119–137. https://doi.org/10.1093/plankt/fbp098

Foreman, R. K., Segura-Noguera, M., & Karl, D. M. (2016). Validation of Ti (III) as a reducing agent in the chemiluminescent determination of nitrate and nitrite in seawater. *Marine Chemistry*, *186*, 83–89. https://doi.org/10.1016/j.marchem.2016.08.003

Fowler, B. L., Neubert, M. G., Hunter-Cevera, K. R., Olson, R. J., Shalapyonok, A., Solow, A. R., & Sosik, H. M. (2020). Dynamics and functional diversity of the smallest phytoplankton on the northeast US shelf. *Proceedings of the National Academy of Sciences*, *117*(22), 12,215–12,221. https://doi.org/10.1073/pnas.1918439117

García, H. E., & Gordon, L. I. (1992). Oxygen solubility in seawater: Better fitting equations. *Limnology and Oceanography*, *37*(6), 1307–1312. https://doi.org/10.4319/lo.1992.37.6.1307

Glover, D. M., Wroblewski, J., & McClain, C. R. (1994). Dynamics of the transition zone in coastal zone color scanner-sensed ocean color in the North Pacific during oceanographic spring. *Journal of Geophysical Research*, *99*(C4), 7501–7511. https://doi.org/10.1029/93JC02144

Guidi, L., Chaffron, S., Bittner, L., Eveillard, D., Larhlimi, A., Roux, S., et al. (2016). Plankton networks driving carbon export in the oligotrophic ocean. *Nature*, *532*(7600), 465–470. https://doi.org/10.1038/nature16942

Hackett, J. D., Anderson, D. M., Erdner, D. L., & Bhattacharya, D. (2004). Dinoflagellates: A remarkable evolutionary experiment. *American Journal of Botany*, *91*(10), 1523–1534. https://doi.org/10.3732/ajb.91.10.1523

Henson, S. A., Sanders, R., & Madsen, E. (2012). Global patterns in efficiency of particulate organic carbon export and transfer to the deep ocean. *Global Biogeochemical Cycles*, *26*, GB1028. https://doi.org/10.1029/2011GB004099

Hirata, T., Hardman-Mountford, N., Brewin, R., Aiken, J., Barlow, R., Suzuki, K., et al. (2011). Synoptic relationships between surface chlorophyll-a and diagnostic pigments specific to phytoplankton functional types. *Biogeosciences*, *8*(2), 311–327. https://doi.org/10.5194/bg-8-311-2011

Holling, C. S. (1966). The functional response of invertebrate predators to prey density. *The Memoirs of the Entomological Society of Canada*, *98*(S48), 5–86. https://doi.org/10.4039/entm9848fv

Holser, R. R., Goni, M. A., & Hales, B. (2011). Design and application of a semi-automated filtration system to study the distribution of particulate organic carbon in the water column of a coastal upwelling system. *Marine Chemistry*, *123*(1–4), 67–77. https://doi.org/10.1016/j.marchem.2010.10.001

Huang, K., Ducklow, H., Vernet, M., Cassar, N., & Bender, M. L. (2012). Export production and its regulating factors in the West Antarctica Peninsula region of the Southern Ocean. *Global Biogeochemical Cycles*, *26*, GB2005. https://doi.org/10.1029/2010GB004028

Juranek, L., Hamme, R. C., Kaiser, J., Wanninkhof, R., & Quay, P. D. (2010). Evidence of O_2 consumption in underway seawater lines: Implications for air-sea O_2 and CO_2 fluxes. *Geophysical Research Letters*, *37*, L01601. https://doi.org/10.1029/2009GL040423

Juranek, L., & Quay, P. (2005). In vitro and in situ gross primary and net community production in the North Pacific Subtropical Gyre using labeled and natural abundance isotopes of dissolved O_2. *Global Biogeochemical Cycles*, *19*, GB3009. https://doi.org/10.1029/2004GB002384

Juranek, L., & Quay, P. (2012). Using triple isotopes of dissolved oxygen to evaluate global marine productivity. *Annual Review of Marine Science*, *5*, 503–524. https://doi.org/10.1146/annurev_marine-121211-172430

Juranek, L., Quay, P., Feely, R., Lockwood, D., Karl, D., & Church, M. (2012). Biological production in the NE Pacific and its influence on air-sea CO_2 flux: Evidence from dissolved oxygen isotopes and O_2/Ar. *Journal of Geophysical Research*, *117*, C05022. https://doi.org/10.1029/2011JC007450

Kaiser, J., Reuer, M. K., Barnett, B., & Bender, M. L. (2005). Marine productivity estimates from continuous O_2/Ar ratio measurements by membrane inlet mass spectrometry. *Geophysical Research Letters*, *32*, L19605. https://doi.org/10.1029/2005GL023459

Karl, D., Christian, J., Dore, J., Hebel, D., Letelier, R., Tupas, L., & Winn, C. (1996). Seasonal and interannual variability in primary production and particle flux at station ALOHA. *Deep-Sea Research Part II: Topical Studies in Oceanography*, *43*(2–3), 539–568. https://doi.org/10.1016/0967-0645(96)00002-1

Kavanaugh, M. T., Emerson, S. R., Hales, B., Lockwood, D. M., Quay, P. D., & Letelier, R. M. (2014). Physicochemical and biological controls on primary and net community production across northeast Pacific seascapes. *Limnology and Oceanography*, *59*(6), 2013–2027. https://doi.org/10.4319/lo.2014.59.6.2013

Kavanaugh, M. T., Hales, B., Saraceno, M., Spitz, Y. H., White, A. E., & Letelier, R. M. (2014). Hierarchical and dynamic seascapes: A quantitative framework for scaling pelagic biogeochemistry and ecology. *Progress in Oceanography*, *120*, 291–304. https://doi.org/10.1016/j.pocean.2013.10.013

Kooijman, S. A. L. M. (2000). *Dynamic energy and mass budgets in biological systems* (Second ed.). Cambridge, UK: Cambridge university press. https://doi.org/10.1017/CBO9780511565403

Kostadinov, T., Siegel, D., & Maritorena, S. (2010). Global variability of phytoplankton functional types from space: Assessment via the particle size distribution. *Biogeosciences*, *7*(10), 3239–3257. https://doi.org/10.5194/bg-7-3239-2010

Lam, P. J., Doney, S. C., & Bishop, J. K. (2011). The dynamic ocean biological pump: Insights from a global compilation of particulate organic carbon, $CaCO_3$, and opal concentration profiles from the mesopelagic. *Global Biogeochemical Cycles*, *25*, GB3009. https://doi.org/10.1029/2010GB003868

Laufkötter, C., Vogt, M., Gruber, N., Aita-Noguchi, M., Aumont, O., Bopp, L., et al. (2015). Drivers and uncertainties of future global marine primary production in marine ecosystem models. *Biogeosciences*, *12*(23), 6955–6984. https://doi.org/10.5194/bg-12-6955-2015

Laws, E. A., Falkowski, P. G., Smith, W. O., Ducklow, H., & McCarthy, J. J. (2000). Temperature effects on export production in the open ocean. *Global Biogeochemical Cycles*, *14*(4), 1231–1246. https://doi.org/10.1029/1999GB001229

Leblanc, K., Quéguiner, B., Diaz, F., Cornet, V., Michel-Rodriguez, M., de Madron, X. D., et al. (2018). Nanoplanktonic diatoms are globally overlooked but play a role in spring blooms and carbon export. *Nature Communications*, *9*(1), 953. https://doi.org/10.1038/s41467-018-03376-9

Legendre, L., & Le Fèvre, J. (1995). Microbial food webs and the export of biogenic carbon in oceans. *Aquatic Microbial Ecology*, *9*(1), 69–77. https://doi.org/10.3354/ame009069

Letelier, R. M., Karl, D. M., Abbott, M. R., & Bidigare, R. R. (2004). Light driven seasonal patterns of chlorophyll and nitrate in the lower euphotic zone of the North Pacific Subtropical Gyre. *Limnology and Oceanography*, *49*(2), 508–519. https://doi.org/10.4319/lo.2004.49.2.0508

Lin, Y., Cassar, N., Marchetti, A., Moreno, C., Ducklow, H., & Li, Z. (2017). Specific eukaryotic plankton are good predictors of net community production in the Western Antarctic Peninsula. *Scientific Reports*, *7*(1), 14845. https://doi.org/10.1038/s41598-017-14109-1

Litchman, E., Klausmeier, C. A., Schofield, O. M., & Falkowski, P. G. (2007). The role of functional traits and trade-offs in structuring phytoplankton communities: Scaling from cellular to ecosystem level. *Ecology Letters*, *10*(12), 1170–1181. https://doi.org/10.1111/j.1461-0248.2007.01117.x

Lockwood, D., Quay, P. D., Kavanaugh, M. T., Juranek, L. W., & Feely, R. A. (2012). High-resolution estimates of net community production and air-sea CO_2 flux in the northeast Pacific. *Global Biogeochemical Cycles*, *26*, GB4010. https://doi.org/10.1029/2012GB004380

Lomas, M. W., & Moran, S. B. (2011). Evidence for aggregation and export of cyanobacteria and nano-eukaryotes from the Sargasso Sea euphotic zone. *Biogeosciences*, *8*(1), 203–216. https://doi.org/10.5194/bg-8-203-2011

Lomnard, F., Boss, E., Waite, A. M., Vogt, M., Uitz, J., Stemman, L., et al. (2019). Globally consistent quantitative observations of planktonic ecosystems. *Frontiers in Marine Science*, *6*, 196.

Luz, B., & Barkan, E. (2000). Assessment of oceanic productivity with the triple-isotope composition of dissolved oxygen. *Science*, *288*(5473), 2028–2031. https://doi.org/10.1126/science.288.5473.2028

Marañón, E., Cermeño, P., López-Sandoval, D. C., Rodríguez-Ramos, T., Sobrino, C., Huete-Ortega, M., et al. (2013). Unimodal size scaling of phytoplankton growth and the size dependence of nutrient uptake and use. *Ecology Letters*, *16*(3), 371–379. https://doi.org/10.1111/ele.12052

Margalef, R. (1979). Life-forms of phytoplankton as survival alternatives in an unstable environment. *Oceanologica Acta*, *1*, 493–509.

Marshall, J., Hill, C., Perelman, L., & Adcroft, A. (1997). Hydrostatic, quasi-hydrostatic, and nonhydrostatic ocean modeling. *Journal of Geophysical Research*, *102*, 5733–5752. https://doi.org/10.1029/96JC02776

Menden-Deuer, S., & Lessard, E. J. (2000). Carbon to volume relationships for dinoflagellates, diatoms, and other protist plankton. *Limnology and Oceanography*, *45*(3), 569–579. https://doi.org/10.4319/lo.2000.45.3.0569

Michaels, A. F., & Silver, M. W. (1988). Primary production, sinking fluxes and the microbial food web, Deep Sea Research Part A. *Oceanographic Research Papers*, *35*(4), 473–490. https://doi.org/10.1016/0198-0149(88)90126-4

Moberg, E. A., & Sosik, H. M. (2012). Distance maps to estimate cell volume from two-dimensional plankton images. *Limnology and Oceanography: Methods*, *10*(4), 278–288.

Mongin, M., Nelson, D. M., Pondaven, P., & Tréguer, P. (2006). Simulation of upper-ocean biogeochemistry with a flexible-composition phytoplankton model: C, N and Si cycling and Fe limitation in the Southern Ocean. *Deep Sea Research Part II: Topical Studies in Oceanography*, *53*(5–7), 601–619. https://doi.org/10.1016/j.dsr2.2006.01.021

Moutier, W., Duforêt-Gaurier, L., Thyssen, M., Loisel, H., Meriaux, X., Courcot, L., et al. (2017). Evolution of the scattering properties of phytoplankton cells from flow cytometry measurements. *PLoS ONE*, *12*(7), e0181180. https://doi.org/10.1371/journal.pone.0181180

Mouw, C. B., Barnett, A., McKinley, G. A., Gloege, L., & Pilcher, D. (2016). Phytoplankton size impact on export flux in the global ocean. *Global Biogeochemical Cycles*, *30*, 1542–1562. https://doi.org/10.1002/2015GB005355

Murphy, J., & Riley, J. P. (1962). A modified single solution method for the determination of phosphate in natural waters. *Analytica Chimica Acta*, *27*, 31–36. https://doi.org/10.1016/S0003-2670(00)88444-5

Olson, R. J., Shalapyonok, A., & Sosik, H. M. (2003). An automated submersible flow cytometer for analyzing pico-and nano-phytoplankton: FlowCytobot. *Deep-Sea Research Part I: Oceanographic Research Papers*, *50*(2), 301–315. https://doi.org/10.1016/S0967-0637(03)00003-7

Pasciak, W. J., & Gavis, J. (1975). Transport limited nutrient uptake rates in Ditylum brightwellii 1. *Limnology and Oceanography*, *20*(4), 604–617. https://doi.org/10.4319/lo.1975.20.4.0604

Passow, U. (2002). Transparent exopolymer particles (TEP) in aquatic environments. *Progress in Oceanography*, *55*(3–4), 287–333. https://doi.org/10.1016/S0079-6611(02)00138-6

Polovina, J. J., Howell, E., Kobayashi, D. R., & Seki, M. P. (2001). The transition zone chlorophyll front, a dynamic global feature defining migration and forage habitat for marine resources. *Progress in Oceanography*, *49*(1–4), 469–483. https://doi.org/10.1016/S0079-6611(01)00036-2

Poulin, F. J., & Franks, P. J. (2010). Size-structured planktonic ecosystems: Constraints, controls and assembly instructions. *Journal of Plankton Research*, *32*(8), 1121–1130. https://doi.org/10.1093/plankt/fbp145

Poulton, A. J., Adey, T. R., Balch, W. M., & Holligan, P. M. (2007). Relating coccolithophore calcification rates to phytoplankton community dynamics: Regional differences and implications for carbon export. *Deep Sea Research Part II: Topical Studies in Oceanography*, *54*(5–7), 538–557. https://doi.org/10.1016/j.dsr2.2006.12.003

Ribalet, F., Berthiaume, C., Hynes, A., Swalwell, J., Carlson, M., Clayton, S., et al. (2019). SeaFlow data v1; high resolution abundance, size, and biomass of small phytoplankton in the North Pacific. *Scientific Data*, *6*(1), 277. https://doi.org/10.1038/s41597-019-0292-2

Richardson, T. L. (2019). Mechanisms and pathways of small-phytoplankton export from the surface ocean. *Annual Review of Marine Science*, *11*, 57–74. https://doi.org/10.1146/annurev-marine-121916-063627

Roden, G. I. (1971). Aspects of the transition zone in the northeastern Pacific. *Journal of Geophysical Research*, *76*(15), 3462–3475. https://doi.org/10.1029/JC076i015p03462

Roden, G. I. (1972). Temperature and salinity fronts at the boundaries of the subarctic-subtropical transition zone in the western Pacific. *Journal of Geophysical Research*, *77*(36), 7175–7187. https://doi.org/10.1029/JC077i036p07175

Savidge, G., Boyd, P., Pomroy, A., Harbour, D., & Joint, I. (1995). Phytoplankton production and biomass estimates in the northeast Atlantic Ocean, May–June 1990. *Deep Sea Research Part I: Oceanographic Research Papers*, *42*(5), 599–617. https://doi.org/10.1016/0967-0637(95)00016-Y

Schlitzer, R. (2000). Applying the adjoint method for biogeochemical modeling: Export of particulate organic matter in the world ocean. *Geophysical Monograph- American Geophysical Union*, *114*, 107–124.

Sheldon, R., Prakash, A., & Sutcliffe, W. Jr. (1972). The size distribution of particles in the ocean. *Limnology and Oceanography*, *17*(3), 327–340. https://doi.org/10.4319/lo.1972.17.3.0327

Sherr, E. B., & Sherr, B. F. (2002). Significance of predation by protists in aquatic microbial food webs. *Antonie Van Leeuwenhoek*, *81*(1), 293–308. https://doi.org/10.1023/A:1020591307260

Sieburth, J. M., Smetacek, V., & Lenz, J. (1978). Pelagic ecosystem structure: Heterotrophic compartments of the plankton and their relationship to plankton size fractions. *Limnology and Oceanography*, *23*(6), 1256–1263. https://doi.org/10.4319/lo.1978.23.6.1256

Siegel, D. A., Buesseler, K. O., Doney, S. C., Sailley, S. F., Behrenfeld, M. J., & Boyd, P. W. (2014). Global assessment of ocean carbon export by combining satellite observations and food-web models. *Global Biogeochemical Cycles*, *28*, 181–196. https://doi.org/10.1002/2013GB004743

Sommer, U., Charalampous, E., Genitsaris, S., & Moustaka-Gouni, M. (2017). Benefits, costs and taxonomic distribution of marine phytoplankton body size. *Journal of Plankton Research*, *39*(3), 494–508.

Sosik, H. M., Futrelle, J., Brownlee, E. F., Peacock, E., Crockford, T., & Olson, R. J. (2016). hsosik/ifcb-analysis: IFCB-Analysis software system, initial formal release at v2 feature stage edited. http://doi.org/10.5281/zenodo.153978

Sosik, H. M., & Olson, R. J. (2007). Automated taxonomic classification of phytoplankton sampled with imaging-in-flow cytometry. *Limnology and Oceanography: Methods*, *5*(6), 204–216.

Strickland, J., & Parsons, T. R. (1972). *A practical handbook of seawater analysis*. Ottawa, Canada: Fisheries Research Board of Canada.

Tang, E. P. (1995). The allometry of algal growth rates. *Journal of Plankton Research*, *17*(6), 1325–1335. https://doi.org/10.1093/plankt/17.6.1325

Teeter, L., Hamme, R. C., Ianson, D., & Bianucci, L. (2018). Accurate estimation of net community production from O_2/Ar measurements. *Global Biogeochemical Cycles*, *32*, 1163–1181. https://doi.org/10.1029/2017GB005874

Uitz, J., Huot, Y., Bruyant, F., Babin, M., & Claustre, H. (2008). Relating phytoplankton photophysiological properties to community structure on large scales. *Limnology and Oceanography*, *53*(2), 614–630.

Verdy, A., Follows, M., & Flierl, G. (2009). Optimal phytoplankton cell size in an allometric model. *Marine Ecology Progress Series*, *379*, 1–12. https://doi.org/10.3354/meps07909

Viviani, D. A., Björkman, K. M., Karl, D. M., & Church, M. J. (2011). Plankton metabolism in surface waters of the tropical and subtropical Pacific Ocean. *Aquatic Microbial Ecology*, *62*(1), 1–12. https://doi.org/10.3354/ame01451

Wanninkhof, R. (2014). Relationship between wind speed and gas exchange over the ocean revisited. *Limnology and Oceanography: Methods*, *12*(6), 351–362.

Ward, B. A. (2015). Temperature-correlated changes in phytoplankton community structure are restricted to polar waters. *PLoS ONE*, *10*(8), e0135581. https://doi.org/10.1371/journal.pone.0135581

Ward, B. A., Dutkiewicz, S., & Follows, M. J. (2014). Modelling spatial and temporal patterns in size-structured marine plankton communities: Top–down and bottom–up controls. *Journal of Plankton Research*, *36*(1), 31–47. https://doi.org/10.1093/plankt/fbt097

Ward, B. A., Dutkiewicz, S., Jahn, O., & Follows, M. J. (2012). A size-structured food-web model for the global ocean. *Limnology and Oceanography*, *57*(6), 1877–1891. https://doi.org/10.4319/lo.2012.57.6.1877

Ward, B. A., & Follows, M. J. (2016). Marine mixotrophy increases trophic transfer efficiency, mean organism size, and vertical carbon flux, proceedings of the National Academy of Sciences. *USA*, *113*(11), 2958–2963. https://doi.org/10.1073/pnas.1517118113

Ward, B. A., Marañón, E., Sauterey, B., Rault, J., & Claessen, D. (2017). The size dependence of phytoplankton growth rates: A trade-off between nutrient uptake and metabolism. *The American Naturalist*, *189*(2), 170–177. https://doi.org/10.1086/689992

West, G. B., Brown, J. H., & Enquist, B. J. (1997). A general model for the origin of allometric scaling laws in biology. *Science*, *276*(5309), 122–126. https://doi.org/10.1126/science.276.5309.122

Westberry, T., Behrenfeld, M., Siegel, D., & Boss, E. (2008). Carbon-based primary productivity modeling with vertically resolved photoacclimation. *Global Biogeochemical Cycles*, *22*, GB2024. https://doi.org/10.1029/2007GB003078

White, A. E., Barone, B., Letelier, R., & Karl, D. M. (2017). Productivity diagnosed from the diel cycle of particulate carbon in the North Pacific subtropical gyre. *Geophysical Research Letters*, *44*, 3752–3760. https://doi.org/10.1002/2016GL071607

White, A. E., Whitmire, A., Barone, B., Letelier, R., Karl, D. M., & Church, M. J. (2015). Phenology of particle size distributions in the North Pacific gyre. *Journal of Geophysical Research: Oceans*, *120*, 7381–7399. https://doi.org/10.1002/2015JC010897

Worden, A. Z., & Not, F. (2008). Ecology and diversity of picoeukaryotes. *Microbial Ecology of the Oceans*, Second Edition, *2*, 159–205.

Wunsch, C., & Heimbach, P. (2007). Practical global oceanic state estimation. *Physica D: Nonlinear Phenomena*, *230*(1–2), 197–208. https://doi.org/10.1016/j.physd.2006.09.040